Heterogeneous & Homogeneous & Bio- & Nano-
CHEMCATCHEM
CATALYSIS

Accepted Article

Title: Ru-Zn/ZrO_2 nanocomposite catalysts fabricated by galvanic replacement for benzene partial hydrogenation

Authors: Gongbing Zhou, Hao Wang, Jing Tian, Yan Pei, Kangnian Fan, Minghua Qiao, Bin Sun, and Baoning Zong

To be cited as: *ChemCatChem* 10.1002/cctc.201701696

Link to VoR: http://dx.doi.org/10.1002/cctc.201701696

A Journal of
ChemPubSoc Europe

WILEY-VCH

www.chemcatchem.org

Ru–Zn/ZrO_2 nanocomposite catalysts fabricated by galvanic replacement for benzene partial hydrogenation

Gongbing Zhou,[a,b] Hao Wang,[a] Jing Tian,[a] Yan Pei,[a] Kangnian Fan,[a] Minghua Qiao,*[a] Bin Sun,[c] and Baoning Zong*[c]

Abstract: A strategy based on galvanic replacement between metallic Zn and Ru salt followed by acid treatment was developed to fabricate the supported Ru–Zn/ZrO_2 nanocomposite catalysts with controlled contents of Zn for benzene partial hydrogenation to cyclohexene. The catalysts were systematically characterized by techniques such as extended X-ray absorption fine structure, X-ray photoelectron spectroscopy, and transmission electron microscopy. In benzene partial hydrogenation, with the decrease in the content of Zn, the turnover frequency (TOF) of benzene increased monotonically, while the selectivity to cyclohexene evolved in a volcanic trend, passing through a maximum of 72%. Kinetic analysis indicated that with the depletion of Zn, the rate constant for benzene hydrogenation to cyclohexene and that for cyclohexene hydrogenation to cyclohexane increased simultaneously, but the extents of the increments were at variance. It is identified that the ratios of the rate constants were in parallel with the change in the selectivity to cyclohexene, which is attributed to the electronic effect of metallic Zn that modifies the interactions of Ru with benzene and cyclohexene.

Introduction

The precursor to nylon-6, ε-caprolactam, is manufactured on a massive scale mainly by the process starting from saturation hydrogenation of benzene to cyclohexane.[1] To obtain the intermediate cyclohexanone, the low-reactivity cyclohexane is directly oxidized by air (Scheme 1a),[2] which is severely plagued by low efficiency and high explosion risk. As an alternative, Asahi Chemical developed a process starting from benzene partial hydrogenation to cyclohexene. Cyclohexene can be easily hydrated to cyclohexanol, which is then dehydrogenated to cyclohexanone (Scheme 1b).[2–4] The process of Asahi Chemical effectively improves the operation safety and saves one-third of hydrogen, which is therefore more environment-friendly. However, the proprietary catalyst for benzene partial hydrogenation is a bimetallic Ru–Zn black containing as high as 90 wt% of noble metal Ru,[5] which greatly undermines the economic attractiveness of this route as compared to the conventional route.

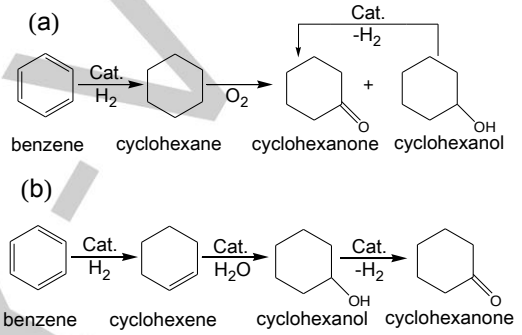

Scheme 1. (a) The conventional route for the production of cyclohexanone starting from the saturation hydrogenation of benzene to cyclohexane, and (b) the route developed by Asahi Chemical for the production of cyclohexanone starting from the partial hydrogenation of benzene to cyclohexene.

Since heterogeneous catalysis occurs on the active sites at the catalyst surface, it is a common practice to transform a bulk catalyst into a supported one to cut down the catalyst cost without reducing the quantity of the active sites exposed.[6] Hence, for benzene partial hydrogenation, many endeavors have been dedicated to the fabrication of supported bimetallic Ru–Zn catalysts and other bimetallic Ru-based catalysts by wetness impregnation,[7] incipient wetness impregnation,[8] co-precipitation,[9] deposition–precipitation,[7,10] "two solvents" impregnation,[11] two-step impregnation,[12] ion-exchange,[13] microemulsion,[14,15] and so on. Recently, galvanic replacement between active metal and the cations of the metal with more positive reduction potential has been utilized to synthesize nanomaterials for biomedical imaging,[16] photothermal cancer treatment,[17] drug delivery,[17] surface-enhanced Raman scattering,[18] and catalysis.[19] Liu et al. found that $Ag_{0.64}Au_{0.36}$@CeO_2 core–shell nanospheres prepared from Ag@CeO_2 by galvanic replacement was 2.5 times more active than Pt@CeO_2 in 4-nitrophenol reduction by ammonia borane.[20] Chen et al. synthesized bimetallic Cu–M/TiO_2 (M = Pt, Pd, Ru, and Rh) catalysts by galvanic replacement between Cu nanoparticles (NPs) and noble metal cations and found that Cu–Pd/TiO_2 catalyzed nitrate reduction with high efficiency.[21] Wu et al. prepared carbon nanotubes-supported Cu–Ru by galvanic replacement between Cu NPs and Ru cations, which showed much higher 1,2-propanediol selectivity in glycerol

[a] Dr. G. Zhou, H. Wang, J. Tian, Dr. Y. Pei, Prof. K. Fan, Prof. Dr. M. Qiao
Collaborative Innovation Center of Chemistry for Energy Materials
Department of Chemistry and Shanghai Key Laboratory of Molecular Catalysis and Innovative Materials
Fudan University
Shanghai 200433 (P.R. China)
E-mail: mhqiao@fudan.edu.cn
[b] Dr. G. Zhou
Key Laboratory of Green Synthesis and Applications
College of Chemistry
Chongqing Normal University
Chongqing 401331 (P.R. China)
[c] Prof. B. Sun, Prof. Dr. B. Zong
State Key Laboratory of Catalytic Materials and Chemical Engineering
Research Institute of Petroleum Processing
SINOPEC
Beijing 100083 (P.R. China)
E-mail: zongbn.ripp@sinopec.com

Supporting information for this article is given via a link at the end of the document.

hydrogenolysis than the Ru catalyst.[22] Song et al. fabricated ultrathin (Pt-enriched cage)@CeO_2 nanostructures by galvanic replacement between K_2PtCl_4 and Ag of Pd@Ag@CeO_2, which led to over 95% conversion and 87% hydrocinnamaldehyde selectivity in cinnamaldehyde hydrogenation.[23] As far as we are aware of, galvanic replacement featured by mild synthetic conditions and high flexibility in composition control has not been utilized in fabricating bimetallic Ru–Zn catalysts for benzene partial hydrogenation to cyclohexene.

In the process of Asahi Chemical, ZrO_2 is added as a dispersant to avoid the aggregation of the Ru–Zn black during the reaction.[5] In the present work, by means of galvanic replacement between the low-cost metallic Zn powders and the Ru salt in the presence of ZrO_2, we successfully developed a new approach to fabricate the bimetallic Ru–Zn/ZrO_2 nanocomposite catalysts for benzene partial hydrogenation. The content of Zn in the Ru–Zn/ZrO_2 catalysts can be finely adjusted by acid post-treatment. The effects of the acid/Zn molar ratios on the composition, structure, and electronic property of the Ru–Zn/ZrO_2 catalysts were systematically investigated. The catalytic activities and selectivities of the Ru–Zn/ZrO_2 catalysts in benzene partial hydrogenation to cyclohexene were evaluated and discussed.

Results and Discussion

Composition and texture

Table 1 summarizes the compositions of the Ru–Zn/ZrO_2(x) nanocomposite catalysts fabricated by galvanic replacement followed by acid treatment, with x representing the nominal HCl/Zn molar ratio. With the increase in the HCl/Zn ratio from 1.32 to 1.85, the Ru content relative to the total catalyst weight maintained virtually constant at around 10 wt%, while the Zn content dropped from 7.44 wt% to 0.53 wt%. The variations in the contents of Ru and Zn are anticipated, as noble metal Ru is resistant to hydrochloric acid, while Zn is vulnerable to acid attack.

Table 1. Physicochemical properties of the ZrO_2 support and the Ru−Zn/ZrO_2(x) nanocomposite catalysts.

Sample	Loading[a] [wt%]		S_{BET}	d_{pore}	V_{pore}	D_{Ru}[b]	S_{Ru}[c]
	Ru	Zn	[$m^2\ g^{-1}$]	[nm]	[$cm^3\ g^{-1}$]	[%]	[$m^2\ g_{Ru}^{-1}$]
ZrO_2	–	–	128	11.7	0.48	–	–
Ru–Zn/ZrO_2(1.32)	9.83	7.44	117	11.7	0.41	2.2	8
Ru–Zn/ZrO_2(1.46)	10.26	3.78	113	12.1	0.42	4.0	15
Ru–Zn/ZrO_2(1.52)	10.27	2.78	118	11.6	0.42	6.2	23
Ru–Zn/ZrO_2(1.85)	10.54	0.53	118	11.5	0.42	7.9	29

[a] Determined by ICP–AES. [b] Dispersion of Ru determined by CO chemisorption. [c] Active surface area of Ru determined by CO chemisorption.

The N_2 adsorption–desorption isotherms of ZrO_2 and the Ru–Zn/ZrO_2(x) nanocomposite catalysts all belong to type IV with H3 hysteresis loop (Figure S1). As summarized in Table 1, the multipoint Brunauer–Emmett–Teller surface area (S_{BET}) of ZrO_2 was 128 $m^2\ g^{-1}$, and its average pore diameter (d_{pore}) and pore volume (V_{pore}) were 11.7 nm and 0.48 $cm^3\ g^{-1}$, respectively. The S_{BET} and V_{pore} of the Ru–Zn/ZrO_2(x) catalysts decreased slightly relative to those of ZrO_2. In addition, there is no significant difference in the textural properties of the catalysts treated with different amounts of hydrochloric acid. However, CO chemisorption disclosed that the dispersion (D_{Ru}) and active surface area (S_{Ru}) of Ru increased monotonically with the increase in the HCl/Zn ratio (Table 1), highlighting the exposure of more Ru surface sites with the leaching of Zn.

Bulk structure and morphology

Figure 1 presents the powder X-ray diffraction (XRD) patterns of ZrO_2 and the Ru–Zn/ZrO_2(x) nanocomposite catalysts. The crystal phase of ZrO_2 is tetragonal (t-ZrO_2, JCPDS 50-1089) in both bare ZrO_2 and the catalysts, and the crystallite sizes of ZrO_2 are all around 7.6 nm, as calculated by the Scherrer equation using the broadening of the t-ZrO_2(0 1 1) peak at 2θ of 30.3°. For the Ru–Zn/ZrO_2(x) catalysts, there is also an additional weak and diffuse feature at *ca.* 44° assignable to the (1 0 1) diffraction of hexagonally close packed (*hcp*) Ru (JCPDS 06-0663).[11] No diffractions from the Zn-containing species were found attributable to the low content and/or the poor crystallinity.

Figure 2 shows the transmission electron microscopy (TEM) images and particle size distribution (PSD) histograms with Gaussian analysis fittings of the catalysts. The average sizes of the Ru–Zn NPs in darker contrast (indicated by arrows) as confirmed by energy-dispersive X-ray spectra (EDX) shown in Figure S2 are 5.8, 5.1, 4.6, and 3.4 nm with the increase in the HCl/Zn ratio, which is qualitatively consistent with the results of CO chemisorption. The change in the particle size is a consequence of the dissolution of Zn (Table 1), which is analogous to our previous finding that the particle size became

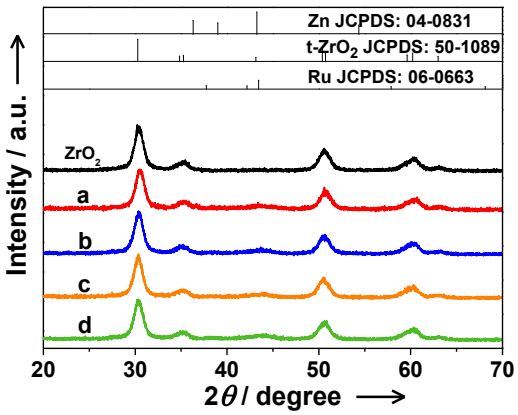

Figure 1. XRD patterns of ZrO_2 and the (a) Ru–Zn/ZrO_2(1.32), (b) Ru–Zn/ZrO_2(1.46), (c) Ru–Zn/ZrO_2(1.52), and (d) Ru–Zn/ZrO_2(1.85) nanocomposite catalysts.

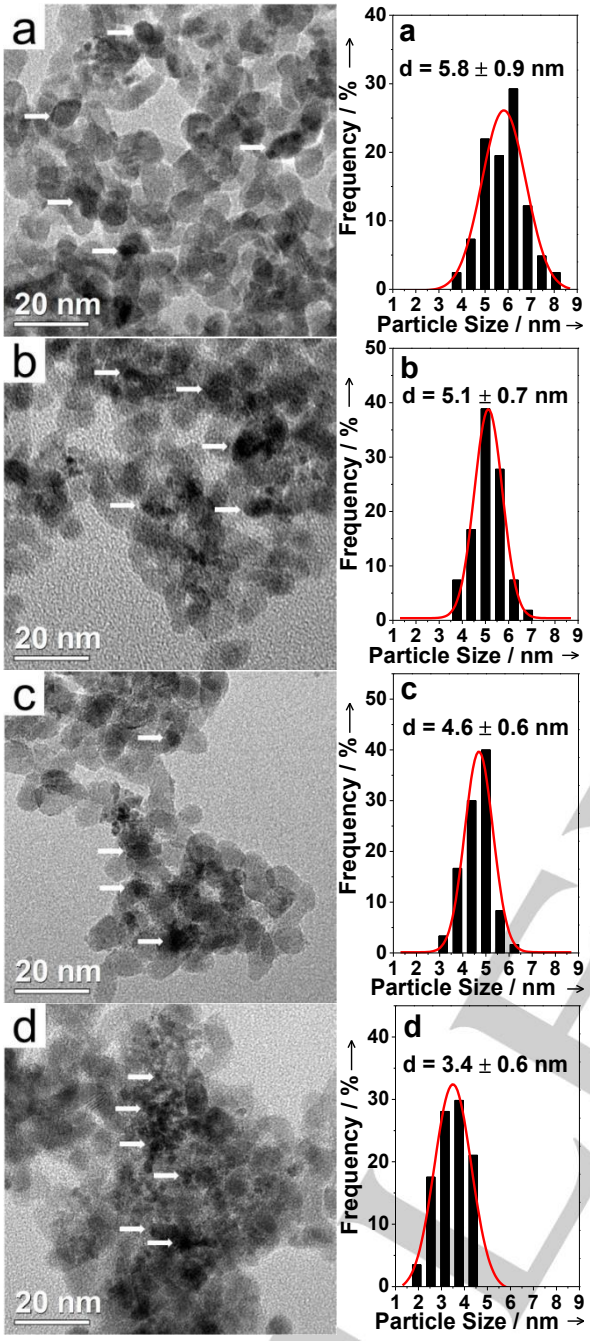

Figure 2. TEM images and particle size distribution histograms with Gaussian analysis fittings of the (a) Ru–Zn/ZrO_2(1.32), (b) Ru–Zn/ZrO_2(1.46), (c) Ru–Zn/ZrO_2(1.52), and (d) Ru–Zn/ZrO_2(1.85) nanocomposite catalysts.

smaller after alkali leaching of Zn in Ru–Zn/ZrO_2 prepared by the deposition–precipitation method.[10] In the high-resolution TEM (HRTEM) images of the catalysts (Figure 3), the lattice fringes from the (0 1 1) planes of *t*-ZrO_2 with the interplanar spacing of ~2.93 Å were clearly observed. The Ru–Zn NPs (marked by ellipses) are irregularly shaped and decreased in size with the increase in the HCl/Zn ratio. However, there are no lattice

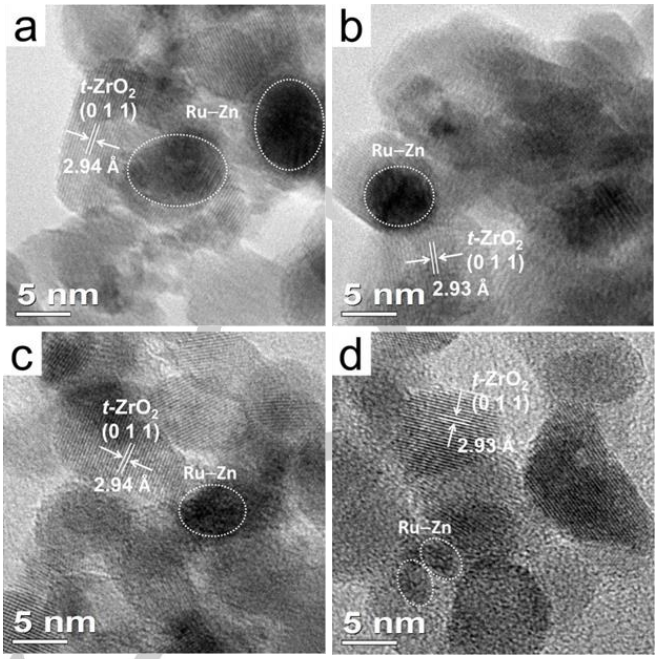

Figure 3. HRTEM images of the (a) Ru–Zn/ZrO_2(1.32), (b) Ru–Zn/ZrO_2(1.46), (c) Ru–Zn/ZrO_2(1.52), and (d) Ru–Zn/ZrO_2(1.85) nanocomposite catalysts.

fringes on the Ru–Zn NPs, inferring their poor crystallinity.

Surface composition and chemical state

The surface compositions of the Ru–Zn/ZrO_2(*x*) nanocomposite catalysts derived from the Ru 3p and Zn 2p X-ray photoelectron spectroscopic (XPS) spectra (Figure 4) and the Zr 3d XPS spectra (Figure S3) are compiled in Table 2. The surface Ru/Zr and Ru/Zn molar ratios are higher than the corresponding bulk ratios, which evidences that Ru was always segregated on the catalysts and complies with the mechanism of galvanic replacement that the newly formed metal atoms are deposited on the surface of the sacrificial metal.[24] The surface Ru/Zr ratio was also found to increase with the HCl/Zn ratio, which indicates the increased dispersion of Ru and is consistent with the CO chemisorption results. In contrast, the surface Zn/Zr ratio decreased with the increase in the HCl/Zn ratio for the leaching of Zn.

Deconvolution of the Zn $2p_{3/2}$ peak In Figure 4 gave two zinc species with the binding energies (BEs) of 1021.8 and 1022.5 eV. Referring to the literature, we assigned the former to metallic Zn[25] while the latter to ZnO.[26] With the increase in the HCl/Zn ratio, the Zn $2p_{3/2}$ peaks of both zinc species were attenuated as expected. On the other hand, with the increase in the HCl/Zn ratio from 1.32 to 1.85, the Ru $3p_{3/2}$ BE shifted steadily from 459.8 to 460.7 eV, both of which are close to the Ru $3p_{3/2}$ BE of metallic Ru at 460.3 eV.[27] This metallic nature of Ru is further substantiated by the resemblance between the Ru K-edge X-ray absorption near-edge structure (XANES) spectra of the catalysts

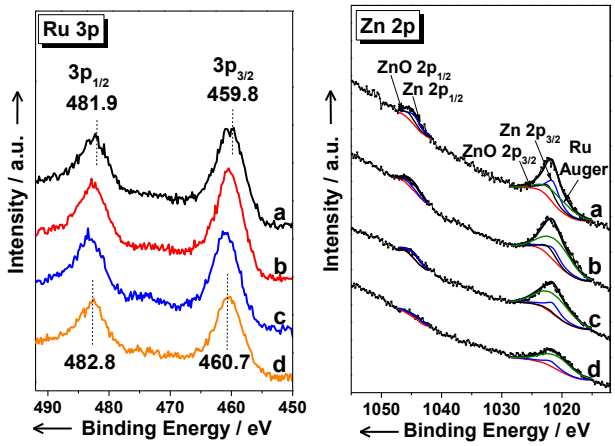

Figure 4. Ru 3p (left) and Zn 2p (right) spectra of the (a) Ru–Zn/ZrO_2(1.32), (b) Ru–Zn/ZrO_2(1.46), (c) Ru–Zn/ZrO_2(1.52), and (d) Ru–Zn/ZrO_2(1.85) nanocomposite catalysts.

Table 2. XPS results of the Ru−Zn/ZrO_2(*x*) nanocomposite catalysts.

Catalyst	Surface molar ratio[a]		
	Ru/Zr	Zn/Zr	Ru/Zn
Ru–Zn/ZrO_2(1.32)	0.26(0.14)	0.048(0.17)	5.43(0.82)
Ru–Zn/ZrO_2(1.46)	0.31(0.15)	0.036(0.08)	8.52(1.88)
Ru–Zn/ZrO_2(1.52)	0.35(0.14)	0.035(0.06)	9.96(2.33)
Ru–Zn/ZrO_2(1.85)	0.42(0.14)	0.027(0.01)	15.5(14.0)

[a] Data in parentheses are the bulk molar ratios determined by ICP–AES.

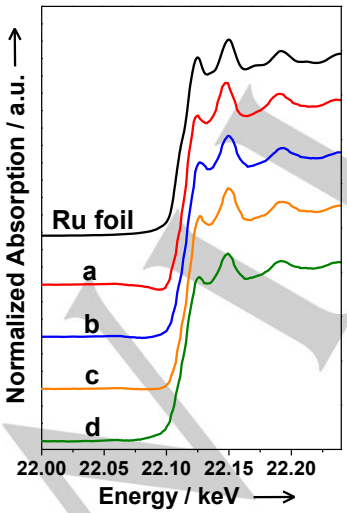

Figure 5. Normalized Ru K-edge XANES spectra of the (a) Ru–Zn/ZrO_2(1.32), (b) Ru–Zn/ZrO_2(1.46), (c) Ru–Zn/ZrO_2(1.52), and (d) Ru–Zn/ZrO_2(1.85) nanocomposite catalysts. The spectrum of the Ru foil is included as a reference.

and that of the Ru foil standard (Figure 5). Regarding that the Pauling electronegativity of Zn (1.65) is lower than that of Ru (2.20), metallic Zn tends to donate electron to Ru. Thus, Ru in the Ru–Zn NPs became less electron-enriched at higher HCl/Zn ratio/lower Zn content, which rationalizes the positive shift of the Ru $3p_{3/2}$ BE observed in Figure 4.

Microstructure

Since XRD and HRTEM did not afford valuable structural information of the Ru–Zn NPs derived from galvanic replacement, extended X-ray absorption fine structure (EXAFS), a powerful and specific tool for probing local atomic structure, was employed to characterize the Ru–Zn/ZrO_2(*x*) nanocomposite catalysts. Figure 6A illustrates the radial distribution functions (RDFs) originated from the Ru K-edge EXAFS data of the catalysts as well as the Ru foil standard. The position of the peak reflects the distance between the central Ru atoms and their neighboring atoms. The main Ru–Ru coordination peaks of the catalysts all appear at 2.36 Å, which is identical to that of the Ru foil standard and the report of Karim *et al.*[28] The attenuation of this peak with the increase in the HCl/Zn

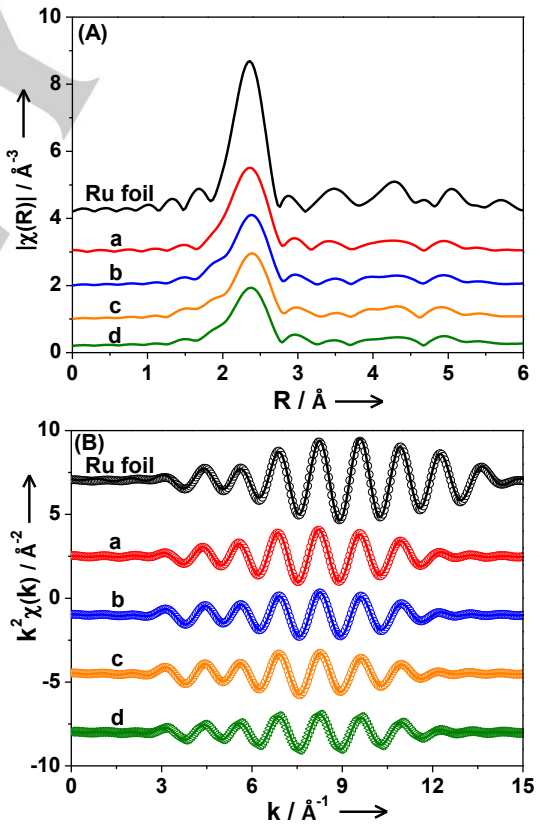

Figure 6. (A) The RDFs after Fourier transformation of the Ru K-edge k^2-weighted $\chi(k)$ data and (B) experimental $k^2\chi(k)$ data (○) and fitted curves (—) of the (a) Ru–Zn/ZrO_2(1.32), (b) Ru–Zn/ZrO_2(1.46), (c) Ru–Zn/ZrO_2(1.52), and (d) Ru–Zn/ZrO_2(1.85) nanocomposite catalysts. The corresponding data of the Ru foil are also presented for reference.

ratio is indicative of the decrease in the Ru–Ru coordination number (CN).

Table 3 summarizes the corresponding structural parameters of the Ru–Zn/ZrO_2(x) nanocomposite catalysts. The reliability of the fitting is confirmed by the good consistency of the simulated $k^2\chi(k)$ curves with the experimental data (Figure 6B). It can be seen from Table 3 that the Ru–Ru CN dropped from 9.3 for Ru–Zn/ZrO_2(1.32) to 5.5 for Ru–Zn/ZrO_2(1.85). Meanwhile, the Ru–Zn CN decreased from 2.9 to 1.1. On the other hand, there were no significant deviations in the Ru–Ru and Ru–Zn distances among the Ru–Zn/ZrO_2(x) catalysts within the error ranges, with the former being close to that of the Ru foil standard, whereas the latter ranged in the Ru–Zn distances of a ternary $HfRu_2Zn_{20}$ intermetallic compound extracted from single crystal XRD data,[29] indicating the alloying between Ru and Zn at least at the interface. It should be mentioned that the fitting results based on k^0- and k^1-weightings afforded similar structural parameters (Tables S1 and S2 and Figures S4 and S5). In conjugation with the elemental analysis (Table 1), TEM/HRTEM (Figures 2 and 3), and XPS results (Figure 4 and Table 2), the synchronous decrease in the Ru–Ru and Ru–Zn CNs can be interpreted as the fracture of larger Ru–Zn NPs to smaller ones and the decrease in the Zn content during the leaching of metallic Zn, respectively.

Table 3. The structural parameters derived from the k^2-weighted curve fittings of the Ru K-edge EXAFS data of the Ru−Zn/ZrO_2(x) nanocomposite catalysts and the Ru foil standard.

Sample	Pair	CN	R [Å]	$\Delta\sigma^2$ [10^{-3} Å^2]	ΔE_0 [eV]
Ru foil	Ru–Ru	11.4 ± 1.0	2.68 ± 0.02	5.00	−3.8
Ru–Zn/ZrO_2(1.32)	Ru–Ru	9.3 ± 0.9	2.69 ± 0.02	3.47	−8.1
	Ru–Zn	2.9 ± 0.3	2.64 ± 0.02	1.88	11.7
Ru–Zn/ZrO_2(1.46)	Ru–Ru	8.3 ± 0.8	2.71 ± 0.02	5.00	−0.5
	Ru–Zn	2.2 ± 0.2	2.63 ± 0.02	4.35	10.1
Ru–Zn/ZrO_2(1.52)	Ru–Ru	7.0 ± 0.7	2.70 ± 0.02	4.13	13.2
	Ru–Zn	1.9 ± 0.2	2.63 ± 0.02	3.00	−4.6
Ru–Zn/ZrO_2(1.85)	Ru–Ru	5.5 ± 0.6	2.71 ± 0.02	6.07	3.9
	Ru–Zn	1.1 ± 0.1	2.64 ± 0.02	3.27	−5.9

Benzene partial hydrogenation

Figure 7 presents the reaction profiles of benzene partial hydrogenation on the Ru–Zn/ZrO_2(x) nanocomposite catalysts. As a typical consecutive reaction, benzene decreased while cyclohexane increased in contents with the reaction time (t). Meanwhile, the content of cyclohexene increased first, passed through a maximum, and then decreased.

Table 4 compiles the corresponding catalytic results. It is

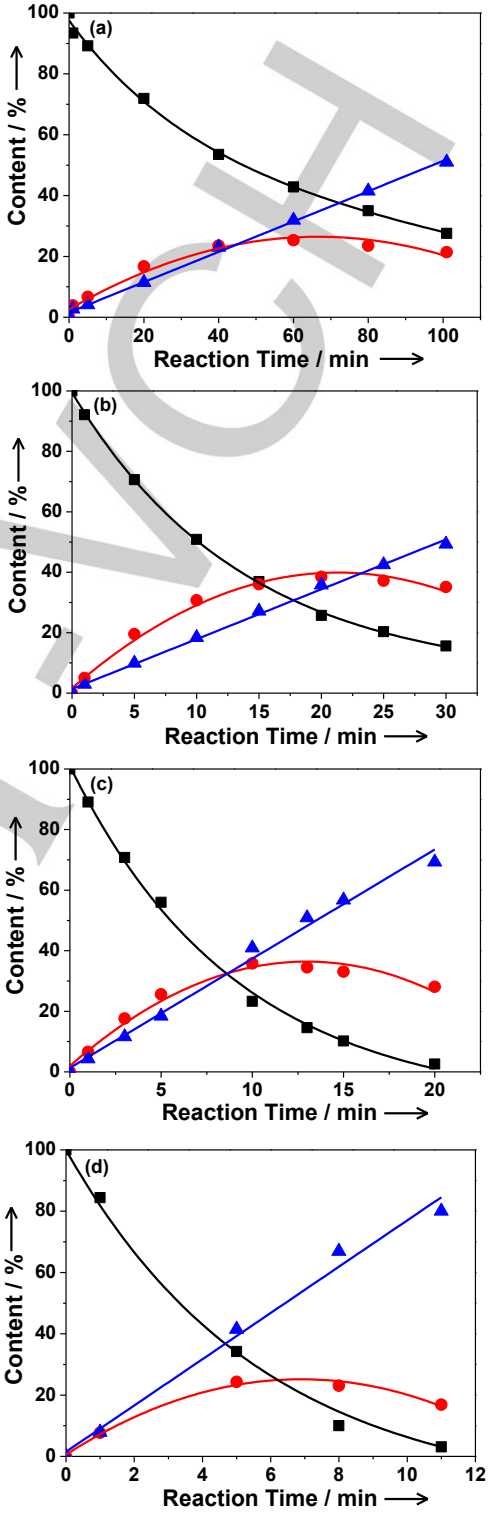

Figure 7. The time courses of benzene hydrogenation over the (a) Ru–Zn/ZrO_2(1.32), (b) Ru–Zn/ZrO_2(1.46), (c) Ru–Zn/ZrO_2(1.52), and (d) Ru–Zn/ZrO_2(1.85) nanocomposite catalysts. Reaction conditions: 1.0 g catalyst, 50 ml benzene, 100 ml H_2O, 2.0 g $ZnSO_4{\cdot}7H_2O$, temperature of 413 K, H_2 pressure of 5.0 MPa, and stirring rate of 1200 rpm. (■) benzene, (●) cyclohexene, and (▲) cyclohexane. Dots: experimental data; lines: fitted curves using the integrated rate equations developed in Ref. 31.

Table 4. Results of benzene partial hydrogenation over the Ru−Zn/ZrO_2(*x*) nanocomposite catalysts.[a]

Catalyst	Conv.[b] [%]	S_{CHE}[b] [%]	Y_{CHE}[b] [%]	t[b] [min]	S_0[c] [%]	r_0[d]	TOF [s^{-1}]
Ru–Zn/ZrO_2(1.32)	57	44	25	60	61	6.7	5.2
Ru–Zn/ZrO_2(1.46)	75	52	39	20	72	29.7	12.2
Ru–Zn/ZrO_2(1.52)	77	47	36	10	66	54.6	14.4
Ru–Zn/ZrO_2(1.85)	90	26	23	8	52	90.0	18.2

[a] Reaction conditions: 1.0 g catalyst, 50 ml benzene, 100 ml H_2O, 2.0 g $ZnSO_4·7H_2O$, temperature of 413 K, H_2 pressure of 5.0 MPa, and stirring rate of 1200 rpm. [b] Values recorded at the maximum yield of cyclohexene. [c] Initial selectivity to cyclohexene. [d] Weight-specific activity, unit in mmol g_{cat}^{-1} min^{-1}.

found that the initial weight-specific activity (r_0) increased steadily with the decrease in the content of Zn. To exclude the effect of the difference in the particle size/dispersion of Ru on the activity, we calculated the turnover frequencies (TOFs) of benzene on the catalysts based on the r_0 and D_{Ru} listed in Table 1. As also shown in Table 4, the TOF displayed the same trend, though not as drastic as that of the r_0, verifying that the intrinsic activities are indeed not identical among the Ru–Zn/ZrO_2(*x*) catalysts.

Benzene partial hydrogenation on the Ru catalysts has been verified as zero order relative to H_2 and first order relative to benzene.[30,31] The latter is readily evidenced on our Ru–Zn/ZrO_2(*x*) nanocomposite catalysts by good linearity between the natural logarithm of the benzene content against *t* (Figure S6), showing that the reaction rate is determined by the coverage of benzene. Since benzene is characterized by an electron-rich delocalized π system (–0.236e per carbon atom), its adsorption is favored on the electron-deficient sites, which is supported by our previous finding that benzene adsorbs more strongly on the positively charged Ru sites than on Ru^0.[32] As demonstrated in Figure 4, when decreasing the content of Zn in the Ru–Zn/ZrO_2(*x*) catalysts, Ru became less electron-enriched, thus promoting the adsorption of benzene and improving the intrinsic activity.

Different from the monotonic increase in the TOF with the decrease in the content of Zn, a volcanic relationship was observed in Table 4 for the initial selectivity to cyclohexene (S_0), which indicates that there is an optimal content of Zn to maximize the selectivity to cyclohexene. The highest S_0 of 72% was obtained on the Ru–Zn/ZrO_2(1.46) catalyst, which outperforms those on the Ru–Cu/ZnO,[7] Ru–Zn/MCM-41,[8] and Ru–Fe/TiO_2 catalysts[33] under similar reaction conditions, demonstrating that galvanic replacement is a promising method to fabricate selective catalyst for the challenging benzene partial hydrogenation reaction. Figure 8 presents the plots of cyclohexene selectivity versus benzene conversion over the Ru–Zn/ZrO_2(*x*) catalysts. It is apparent that the Ru–Zn/ZrO_2(1.46) catalyst was more selective than others in the whole reaction process. It should be noted that the productivity of cyclohexene on the Ru–Zn/ZrO_2(1.46) catalyst was 107 mmol

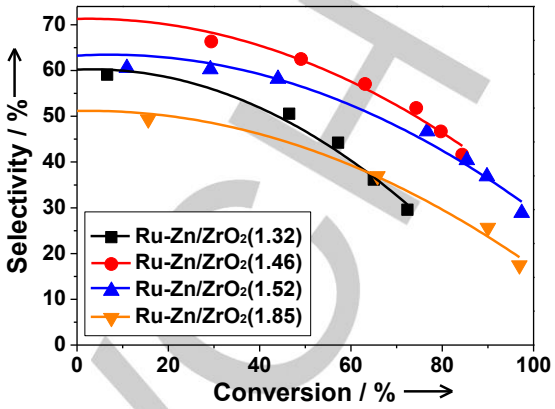

Figure 8. Plots of the selectivity towards cyclohexene versus the conversion of benzene over the Ru−Zn/ZrO_2(*x*) nanocomposite catalysts.

g_{Ru}^{-1} min^{-1}, which is more than 5 times of that on the proprietary bimetallic Ru–Zn black catalyst (19 mmol g_{Ru}^{-1} min^{-1})[5], verifying the higher efficiency of the Ru–Zn/ZrO_2(1.46) catalyst fabricated by galvanic replacement in utilizing noble metal Ru.

It has been elucidated by first-principles calculations that the hydrogenatin of benzene is more difficult than that of cyclohexene over Ru, since the activation barrier for the hydrogenation of the latter is much lower than that of the former[34]. This theoretical prediction is substantiated in Figure 9a by the finding that the rate constant k_1 for benzene hydrogenation to cyclohexene (the first step) is always lower than the rate constant k_2 for cyclohexene hydrogenation to cyclohexane (the second step) over the Ru–Zn/ZrO_2(*x*) nanocomposite catalysts. The k_1 and k_2 values were derived from the fitting of the reaction profiles in Figure 7 using the integrated rate equations for benzene partial hydrogenation over Ru.[31] Furthermore, Figure 9a shows that with the decrease in the content of Zn, both k_1 and k_2 increased, but the extents of the increments are not identical. When the content of Zn was reduced from 7.44 wt% to 3.78 wt%, k_1 increased faster than k_2. Further reducing the content of Zn led to a faster increase of k_2 than k_1. As a result, the k_1/k_2 ratio increased from 0.54 to 0.79 first, and then decreased steadily to 0.41, which is nicely in parallel with the evolution of S_0 (Figure 9b).

The above results indicate that Zn can modify the reaction kinetics of both steps in benzene partial hydrogenation. Although the detailed working mechanism of Zn awaits further elucidation, the kinetic data in Figure 9 highlight that, analogous to the first step, the second step is also favored on the less electron-enriched Ru sites. This deduction is reasonable, considering that the C=C double bond in cyclohexene is also highly abundant in electron (–0.494e per carbon atom). Thus, cyclohexene is inclined to adsorb more strongly on the less electron-enriched Ru sites. As evidenced in Figure S7, the maximum desorption temperature for cyclohexene shifted noticeably from 459 K on

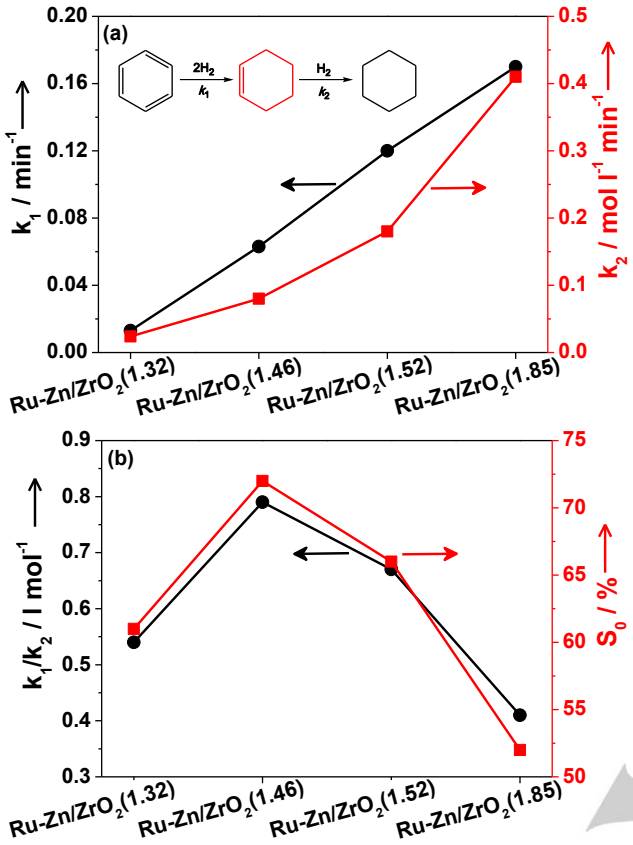

Figure 9. (a) The rate constants for the hydrogenation of benzene to cyclohexene (k_1) and the hydrogenation of cyclohexene to cyclohexane (k_2), and (b) the k_1/k_2 ratios and the S_0 values over the Ru–Zn/ZrO$_2$ nanocomposite catalysts. The rate constants were derived from the reaction data in Figure 7 on the basis of the kinetic equations raised in Ref. 31.

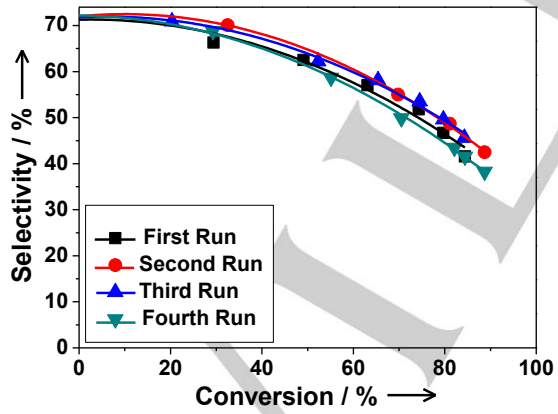

Figure 10. Comparison of cyclohexene selectivity versus benzene conversion over the Ru–Zn/ZrO$_2$(1.46) nanocomposite catalyst from the first run to the fourth run in benzene partial hydrogenation.

the Ru–Zn/ZrO$_2$(1.32) catalyst to 513 K on the Ru–Zn/ZrO$_2$(1.85) catalyst. Since the first step is responsible for the production of cyclohexene, while the second step is responsible for the consumption of cyclohexene, and both steps are promoted on the less electron-enriched Ru sites, it is expected that to maximize the cyclohexene selectivity an optimal content of Zn is needed to render a best compromise between the two steps.

In view of the distinguished catalytic performance of the Ru–Zn/ZrO$_2$(1.46) catalyst, its stability was examined; the results are illustrated in Figure 10. After each catalytic testing, the organic phase was separated by suction, and the aqueous mixture containing the catalyst and $ZnSO_4$ was used in a successive cycle without further treatment. It was found that the cyclohexene selectivity versus benzene conversion curve of the fourth run was still similar to that of the first run, highlighting that there was no significant change in the nature of the catalyst. The excellent stability of the Ru–Zn/ZrO$_2$(1.46) catalyst was further substantiated by the virtually identical morphology and PSD between the as-prepared Ru–Zn/ZrO$_2$(1.46) catalyst (Figure 3b) and the catalyst after the fourth run (Figure S8).

Conclusions

The supported Ru–Zn/ZrO$_2$ nanocomposite catalysts were fabricated by the galvanic replacement strategy that has the merits of mild preparation conditions and versatility in composition control. In benzene partial hydrogenation to cyclohexene, by finely tuning the content of Zn in the catalysts by acid post-treatment, we successfully obtained the Ru–Zn/ZrO$_2$(1.46) catalyst displaying high cyclohexene selectivity and excellent stability. The existence of an appropriate amount of Zn is critical to the high selectivity. This work affords a feasible and promising strategy to the fabrication of the cost-effective and selective catalyst for the highly challenging but industrially significant reaction of benzene partial hydrogenation to cyclohexene.

Experimental Section

Preparation

The chemicals, if not specified, were supplied by Sinopharm Chemical Reagent and of analytical grade (A.R.). The gases were purchased from Shanghai Youjiali Liquid Helium. ZrO$_2$ was synthesized according to our previous work with slight modification.[30] Namely, the ammonia solution (25–28 wt%) was added dropwise to an aqueous solution of $ZrOCl_2{\cdot}8H_2O$ (0.50 mol L^{-1}) under vigorous stirring at room temperature until the pH of 10. After being refluxed at 373 K for 24 h, the resulting precipitates were separated by centrifugation, re-slurried, washed with deionized water until neutrality and removal of the chloride ions by $AgNO_3$ test. The precipitates were dried at 373 K for 24 h, and then calcined at 873 K for 5 h at a heating rate of 10 K min^{-1}.

The bimetallic Ru–Zn/ZrO$_2$ nanocomposite catalysts were fabricated by galvanic replacement, as illustrated in Scheme 2. Specifically, one gram of the as-synthesized ZrO$_2$, 0.50 g of Zn powders (200 meshes), and 5.0 ml of deionized water were mixed together and stirred at 363 K. Then, 3.0 ml of 0.40 M aqueous solution of $RuCl_3{\cdot}3H_2O$ (A.R., Shanghai Aoke), corresponding to a nominal Ru content relative to ZrO$_2$ of 12.0 wt%, were

added dropwise to the slurry and stirred for another 5 min. The nominal Zn/Ru^{3+} molar ratio was 6.48 to guarantee the entire reduction of Ru. The reaction during galvanic replacement was $3Zn + 2Ru^{3+} = 3Zn^{2+} + 2Ru$, as the standard reduction potential of the Zn^{2+}/Zn couple (–0.76 V versus the standard hydrogen electrode, SHE) is much lower than that of the Ru^{3+}/Ru couple (0.68 V versus SHE). After galvanic replacement, aside from residual metallic Zn combining with Ru, there were also oxidized zinc species arising from the hydrolysis of Zn^{2+} or the oxidation of metallic Zn by dissolved oxygen.[35] Hence, the black slurry was cooled down to room temperature, and hydrochloric acid (37%) was added dropwise under mild stirring to adjust the content of metallic Zn and also to remove the oxidized zinc species that might cover the catalyst by reactions of $Zn + 2HCl = ZnCl_2 + H_2$ and $ZnO + 2HCl = ZnCl_2 + H_2O$, respectively. Finally, the solids were washed with deionized water until neutrality and removal of the chloride ions by $AgNO_3$ test. Surface analysis by XPS also confirmed that Cl was absent. The as-prepared nanocomposite catalysts were denoted as $Ru–Zn/ZrO_2(x)$, where x represents the nominal HCl/Zn molar ratio of 1.32, 1.46, 1.52, or 1.85.

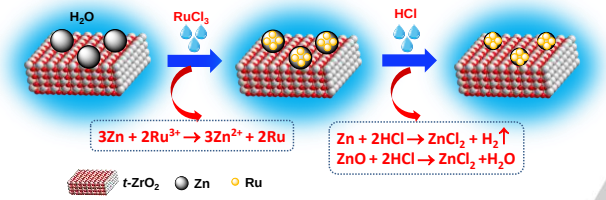

Scheme 2. Illustration of the formation process of the $Ru–Zn/ZrO_2$ nanocomposite catalysts via galvanic replacement followed by acid treatment.

Catalytic testing

Partial hydrogenation of benzene was conducted in a 500 ml Hastelloy autoclave stirred mechanically. After charging 1.0 g of catalyst, 100 ml of H_2O, 2.0 g of $ZnSO_4·7H_2O$, and 50 ml of benzene, the autoclave was sealed and purged with H_2 several times to expel air. The reaction conditions were the temperture of 413 K, the H_2 pressure of 5.0 MPa, and the stirring rate of 1200 rpm, which are typical for this reaction.[3,4,7–15] During the reaction, a small aliquot of the sample was discharged from the autoclave at intervals and analyzed on a GC122 gas chromatograph fitted with a thermal conductivity detector (TCD) and a PEG-20M stainless steel packed column. The catalysts were evaluated at least in duplicate, and the results from replicate runs agreed to within ±2%.

The TOF of benzene and the S_0 of cyclohexene were used to denote the activity and selectivity of the catalyst, respectively. For the calculation of the TOF, the r_0, *i.e.*, the moles of benzene converted per gram of the catalyst per minute at zero reaction time (t), was obtained first by referring to the procedures proposed previously.[36] To figure out r_0, a polynomial equation was used to fit the benzene content–t curve. Then, the equation was differentiated, and r_0 was obtained by substituting zero for t. The TOF was calculated using the equation of $TOF = r_0 \times M_{Ru}/(D_{Ru} \times W)$,[30] where M_{Ru} was the molar mass of Ru, and W was the loading of Ru. The S_0 was acquired through the extrapolation of the fitted cyclohexene selectivity–t curve to t of zero.

Acknowledgements

This work was supported by the National Key R&D program of China (2016YFB0301600), the NSF of China (21373055, 21703024), the Science & Technology Commission of Shanghai Municipality (08DZ2270500), the Beijing Synchrotron Radiation Facility (BSRF), the SINOPEC (S411063), the Scientific and Technological Research Program of Chongqing Municipal Education Commission (KJ1500305), and the Science & Technology Commission of Chongqing Municipality (cstc2016jcyjA0392).

Keywords: Galvanic replacement • Ru–Zn • benzene • hydrogenation • cyclohexene

[1] L. Lloyd, *Handbook of Industrial Catalysis* Springer, New York, **2011**.
[2] K. Weissermel, H. J. Arpe, *Industrial Organic Chemistry, 4th ed.* Wiley-VCH, Weinheim, **2003**.
[3] L. Foppa, J. Dupont, *Chem. Soc. Rev.* **2015**, *44*, 1886–1897.
[4] Y. Pei, G. B. Zhou, N. Luan, B. N. Zong, M. H. Qiao, F. Tao, *Chem. Soc. Rev.* **2012**, *41*, 8140–8162.
[5] H. Nagahara, M. Konishi, Eur. Patent 220525, **1986**.
[6] J. A. Anderson, M. F. García, *Supported Metals in Catalysis* Imperial College Press, London, **2005**.
[7] H. Z. Liu, S. G. Liang, W. T. Wang, T. Jiang, B. X. Han, *J. Mol. Catal. A* **2011**, *341*, 35–41.
[8] T. T. Zhang, Z. M. Wang, Q. Q. Zhao, F. Li, W. Xue, *J. Nanomater.* **2015**, *2015*, 1–8.
[9] J. Q. Wang, Y. Z. Wang, S. H. Xie, M. H. Qiao, H. X. Li, K. N. Fan, *Appl. Catal. A* **2004**, *272*, 29–36.
[10] G. B. Zhou, X. H. Tan, Y. Pei, K. N. Fan, M. H. Qiao, B. Sun, B. N. Zong, *ChemCatChem* **2013**, *5*, 2425–2435.
[11] J. L. Liu, L. J. Zhu, Y. Pei, J. H. Zhuang, H. Li, H. X. Li, M. H. Qiao, K. N. Fan, *Appl. Catal. A* **2009**, *353*, 282–287.
[12] X. H. Yan, Q. Zhang, M. Q. Zhu, Z. B. Wang, *J. Mol. Catal. A* **2016**, *413*, 85–93.
[13] P. Zhang, T. B. Wu, T. Jiang, W. T. Wang, H. Z. Liu, H. L. Fan, Z. F. Zhang, B. X. Han, *Green Chem.* **2013**, *15*, 152–159.
[14] W. Xue, Y. Song, Y. J. Wang, D. D. Wang, F. Li, *Catal. Commun.* **2009**, *11*, 29–33.
[15] S. U. Nandanwar, A. A. Dabbawala, M. Chakraborty, H. C. Bajaj, S. Mukhopadhyay, K. T. Shenoy, *Res. Chem. Intermed.* **2016**, *42*, 1557–1569.
[16] S. J. Bao, S. N. Huang, Y. Liu, Y. R. Hu, W. P. Wang, M. F. Ji, H. L. Li, N. X. Zhang, C. Z. Song, S. F. Duan, *Nanoscale* **2017**, *9*, 7284–7296.
[17] P. S. Zangabad, M. Karimi, F. Mehdizadeh, H. Malekzad, A. Ghasemi, S. Bahrami, H. Zare, M. Moghoofei, A. Hekmatmanesh, M. R. Hamblin, *Nanoscale* **2017**, *9*, 1356–1392.
[18] J. Reguera, J. Langer, D. J. de Aberasturi, L. M. Liz-Marzán, *Chem. Soc. Rev.* **2017**, *46*, 3866–3885.
[19] A. G. M. da Silva, T. S. Rodrigues, S. J. Haigh, P. H. C. Camargo, *Chem. Commun.* **2017**, *53*, 7135–7148.
[20] D. P. Liu, W. Li, X. L. Feng, Y. Zhang, *Chem. Sci.* **2015**, *6*, 7015–7019.
[21] S. Chen, H. Y. Zhang, L. Y. Wu, Y. F. Zhao, C. L. Huang, M. F. Ge, Z. M. Liu, *J. Mater. Chem.* **2012**, *22*, 9117–9122.
[22] Z. J. Wu, Y. Z. Mao, X. X. Wang, M. H. Zhang, *Green Chem.* **2011**, *13*, 1311–1316.
[23] S. Y. Song, X. C. Liu, J. Q. Li, J. Pan, F. Wang, Y. Xing, X. Wang, X. G. Liu, H. J. Zhang, *Adv. Mater.* **2017**, *29*, doi: 10.1002/adma.201700495.
[24] X. H. Xia, Y. Wang, A. Ruditskiy, Y. N. Xia, *Adv. Mater.* **2013**, *25*, 6313–6333.

[25] J. F. Moulder, W. F. Stickle, P. E. Sobol, K. D. Bomben in *Handbook of X-ray Photoelectron Spectroscopy* (Ed: J. Chastain), Perkin-Elmer, Minnesota, **1992**, p. 242.

[26] S. W. Gaarenstroom, N. Winograd, *J. Chem. Phys.* **1977**, *67*, 3500–3506.

[27] P. S. Campbell, C. C. Santini, F. Bayard, Y. Chauvin, V. Collière, A. Podgoršek, M. F. C. Gomes, J. Sá, *J. Catal.* **2010**, *275*, 99–107.

[28] A. M. Karim, V. Prasad, G. Mpourmpakis, W. W. Lonergan, A. I. Frenkel, J. G. Chen, D. G. Vlachos, *J. Am. Chem. Soc.* **2009**, *131*, 12230–12239.

[29] N. Gross, T. Nasch, W. Jeitschko, *J. Solid State Chem.* **2001**, *161*, 288–293.

[30] G. B. Zhou, Y. Pei, Z. Jiang, K. N. Fan, M. H. Qiao, B. Sun, B. N. Zong, *J. Catal.* **2014**, *311*, 393–403.

[31] S. C. Liu, Y. Q. Guo, X. L. Yang, Y. L. Ji, G. Luo, *Chin. J. Catal.* **2003**, *24*, 42–46.

[32] G. B. Zhou, R. F. Dou, H. Z. Bi, S. H. Xie, Y. Pei, K. N. Fan, M. H. Qiao, B. Sun, B. N. Zong, *J. Catal.* **2015**, *332*, 119–126.

[33] J. W. da-Silva, A. J. G. Cobo, *Appl. Catal. A* **2003**, *252*, 9–16.

[34] C. Fan, Y. A. Zhu, X. G. Zhou, Z. P. Liu, *Catal. Today* **2011**, *160*, 234–241.

[35] K. Y. Niu, S. A. Kulinich, J. Yang, A. L. Zhu, X. W. Du, *Chem. Eur. J.* **2012**, *18*, 4234–4241.

[36] S. C. Hu, Y. W. Chen, *Ind. Eng. Chem. Res.* **1997**, *36*, 5153–5159.

10.1002/cctc.201701696

WILEY-VCH

Entry for the Table of Contents

FULL PAPER

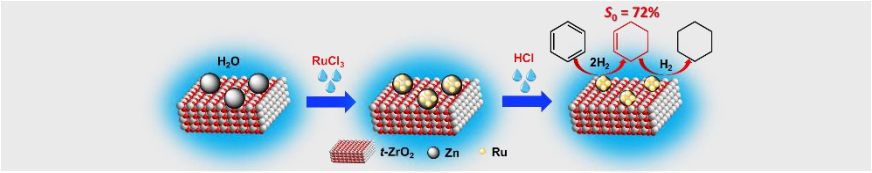

A novel strategy based on galvanic replacement between metallic Zn and Ru salt followed by acid treatment was developed to fabricate the bimetallic Ru–Zn/ZrO_2 nanocomposite catalysts with controlled Zn contents, which exhibited high cyclohexene selectivity and excellent stability in the challenging but industrially significant reaction of benzene partial hydrogenation.

Gongbing Zhou, Hao Wang, Jing Tian, Yan Pei, Kangnian Fan, Minghua Qiao, Bin Sun, Baoning Zong**

Page No. – Page No.

Ru–Zn/ZrO_2 nanocomposite catalysts fabricated by galvanic replacement for benzene partial hydrogenation